Available online at www.sciencedirect.com
SCIENCE DIRECT®
Journal of Solid State Chemistry 177 (2004) 2591–2599
JOURNAL OF SOLID STATE CHEMISTRY
http://elsevier.com/locate/jssc

On the ordering in new low gap semiconductors: PtSnS, PtSnSe, PtSnTe. Experimental and DFT studies

Richard Weihrich,[a,b,*] Daniel Kurowski,[a] Andrea C. Stückl,[a] Samir F. Matar,[b] Franz Rau,[a] and Thomas Bernert[a]

[a] *Institut für Anorganische Chemie, Universität Regensburg, Universitätsstraße 31, Regensburg 93040, Germany*
[b] *Institut de Chimie de la Matière Condensée de Bordeaux, I.C.M.C.B-CNRS, 87, Avenue du Docteur Albert Schweitzer, Pessac Cedex F-33608, France*

Received 11 December 2003; received in revised form 17 March 2004; accepted 21 March 2004

Dedicated to Prof. emer. Dr. Klaus-Jürgen Range on the occasion of his 65th birthday

Abstract

The crystallographic and electronic structures of PtSnS, PtSnSe and PtSnTe were investigated by X-ray structure analysis and density functional theory (DFT) calculations. Conductivity measurements and diffraction patterns show semiconducting ordered pyrite type related compounds containing SnX (X = S, Se, Te) entities. A scheme is presented to model ordered variants according to the relative orientation of the XY dumbbells. It represents the ullmannite, the cobaltite and a new rhombohedral structure type. The scheme allows for a systematic investigation of ordering preferences from first principles. According to the total electronic energy PtSnTe and PtSnSe prefer the cobaltite, PtSnS the rhombohedral structure type. The structural and electronic properties agree with experimental results. The three compounds are predicted to be narrow gap indirect semiconductors from conductivity measurements and band structure calculations.

Keywords: Platinum chalcogenide semiconductors; Pyrite structure; Ordering variants; Electronic structure

1. Introduction

MXY compounds of platinum group metals M and main group IV, V, and VI elements (M–V–V, M–V–VI, and M–IV–VI) turn out to represent fascinating features of the pyrite (FeS_2, space group $Pa\bar{3}$, $C2$) type structural family, concerning crystallographic and electronic structure engineering [1–4]. This is due to the presence of $X-X$ and $X-Y$ dumbbells, related ordering phenomena, and semiconductor to metal transitions. Two PTS related ordered structure types containing XY dumbbells are known represented by the minerals ullmannite (cubic, NiSbS, $P2_13$) and cobaltite (orthorhombic, CoAsS, $Pca2_1$). As shown in this work, they differ only in the relative orientation of XY dumbbells that allows for systematic *ab initio* investigations. Keeping these facts in mind it is surprising that relatively few studies are known on the pyrite-type related Pt-systems and their electronic structures.

From earlier and recent investigations [1,2] on Pd$PnCh$ and Pt$PnCh$ systems with chalcogen and pnictogen elements (Ch = S, Se, Te; Pn = P, As, Sb), we know that these compounds crystallize in the cobaltite and ullmannite structure types. The relation between PtPn_2 and PtXCh is given by replacing Pn_2 dumbbells by XCh. Cobaltite and ullmannite represent two different schemes containing heteroatomic $X-Y$ units. Thus, $MPnCh$ are closer related to the dipnictides MPn_2 (M = Pd, Pt) that crystallize in the cubic pyrite type structure (subsequently as PTS) [5,6]), than to the chalcogenides PtCh_2 that exhibit layered structures. However, due to the occurrence of unpaired electrons the $MPnCh$ systems show metallic conductivity.

PtChX (X = Si, Ge) [7] were also estimated to exhibit ordering of Ch and X. They are isoelectronic to the semiconducting PtPn_2 [3,4]. Comparing Pt–IV–VI and Pt–V–VI compositions different ordering variants are observed. While PtAsS crystallizes in the cubic

*Corresponding author. Fax: +0049-941-9434983.
E-mail address: richard.weihrich@chemie.uni-regensburg.de (R. Weihrich).

0022-4596/$ - see front matter © 2004 Elsevier Inc. All rights reserved.
doi:10.1016/j.jssc.2004.03.031

ullmannite structure [1], Pt*XCh* compounds were found to crystallize in the orthorhombic cobaltite type structure. These contain $X-Y$ (X=Si, Ge; Y=S, Se) dumbbells. For the Sn containing homologues the natural occurrence of a mineral PtSnS was recently reported [8,9] without further structural investigation. Earlier it was estimated to crystallize in the ullmannite (NiSbS) type structure [10]. Another variant containing XY entities was reported as a low temperature structure of PtSiTe with a double c-axis [11]. Inevitably the question arises why and when nature prefers one of the ordering variants.

In the present paper we report on the synthesis and properties of PtSnSe and PtSnTe for the first time and compare it to investigations on synthetic PtSnS. From X-ray data and considerations on the ordering we derive a simple occupation scheme. This allows modelling PtSnS, PtSnSe and PtSnTe from first principles. The model evidences that a new rhombohedral structure is derived in the same way form the PTS as cobaltite and ullmannite. From DFT calculations the crystal and electronic structures are predicted. A comparison is drawn to experimental data in terms of the cell parameters, the electrical conductivity and diffraction patterns.

2. Applied methods

2.1. Experimental

PtSnS, PtSnSe and PtSnTe were synthesized from the elements by high temperature solid state reactions. Equimolar amounts of pure Pt, Sn and the respective chalcogenide Se or Te were heated in sealed and evacuated quartz tubes to 1000°C, 1070°C, and 980°C for PtSnS, PtSnSe, and PtSnTe, respectively. The tubes were quenched after one week. Pulverized samples were investigated by X-ray diffraction with Cu radiation on a Stoe diffractometer. A range of 2θ values from 9° to 90° was measured in steps of 0.02°. For the conductivity measurements powdered samples were pressed to a pellet with 8 mm diameter and 0.5 mm thickness. The pellet was annealed at 300°C for one day. We used the van der Pauw method to measure the dc-conductivity in a temperature range from 8 to 325 K.

2.2. Computing

The structure optimizations were performed with a first principles plane-wave code [12], which treats exchange and correlation in the local density approximation (LDA) of the density functional theory (DFT). Herein the interaction of the valence electrons with ionic cores is described by the use of Vanderbilt ultrasoft non-local pseudopotentials [13] including scalar relativistic corrections and one electron pseudo-orbitals that are expanded over a finite basis set of plane waves. The matrix digitalization was performed by a preconditioned band by band conjugate gradient (CG) algorithm and the update of the charge density by an improved Pulay mixing [14]. For all cell geometry optimizations including the ionic coordinates, volume and shape of the unit cell the conjugate-gradient algorithm was applied. The exchange and correlation potentials of the LDA as implemented in [12] are employed for all calculations. To ensure high performance with respect to the reciprocal space integration we used grids varying from $4\times4\times4$ to $10\times10\times10$ for the sampling of special points on a Monkhorst-Pack net [15]. The k-points were determined by the Bloechl tetrahedron method [16]. The code allows for an increasing level of accuracy by the use of the PREC tag that also varies the cutoff energy. With the highest precision we applied an approach that has been proven for calculations on a series of transition metal chalcogenides [17,18]. Recently, we applied the method for crystal modelling including pyrite type compounds (see e.g. [6]).

Band structures and site-projected density of states were calculated on the optimized structures with a FP-LAPW code [19] using again LDA exchange and correlation functionals [20]. The muffin tin radii were optimized to the structures, as well as the number of k-points (>1000 points per cell) with respect to convergence of the total energy. The modelling and symmetry determinations were carried out applying a commercial simulation package [21].

3. Experimental results

3.1. Physical properties

PtSnS and PtSnSe were received as dark polycrystallites, PtSnTe as a black powder. The melting points were found at 1109.13°C (PtSnSe) and 1005.59°C (PtSnTe). Fig. 1 shows the specific resistivity (ρ) of PtSnSe against the temperature. We observe the resistivity curve of a

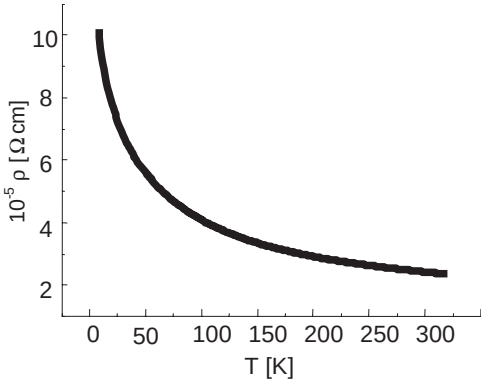

Fig. 1. Resistivity versus temperature for PtSnSe.

semiconductor (decreasing resistivity with increasing temperature). With a specific resistivity of 10^{-4}–$10^{-5}\,\Omega$ cm for 8–300 K the found value is lower than in PtGeSe (0.008 Ω cm [32]).

3.2. X-ray powder diffraction

From X-ray powder diffraction (Fig. 2) patterns are received that are expected for pyrite type related compounds as found for the isoelectronic PtGeX. To derive information on ordering variants we focus on two observations: (i) the occurrence of reflections that indicate ordering in terms of symmetry reduction, and (ii) the splitting of reflections that indicate deviations from the cubic metrics.

The diffraction pattern of PtSnS can be indexed assuming a cubic cell of 6.11 Å. However, the occurrence of the (110) reflection forbids a disordered pyrite structure and the occurrence of the (100) reflection is forbidden for centered structures like the cubic ullmannite. Thus, the symmetry must be lower, but we do not observe the splittings expected for a cobaltite type structure. Broadening of reflections is only observed at higher angles as well as a small splitting of the (440) reflection at $\Theta = 91°$. As easily modelled, this can be due to very small orthorhombic distortions but also to a rhombohedral distortion with a rhombohedral angle of 90.09°. This corresponds to the primitive setting of a hexagonal cell with $a = 8.64$ Å and $c = 10.57$ Å. In the case of PtSnSe, we also observe the (100) and (110) reflections, but here splitting is clearly found for the (200) and higher reflections. This is indicated by the inlets of Fig. 2. The indexing can be performed for an orthorhombic cell with small deviations for a, b and c. This is analogous to the previous observations for PtXY (X = Si, Ge; Y = S, Se) [22], where the lattice distortions were related to the cobaltite structure. For PtSnTe we do not observe a splitting of the (200), but of higher reflections. Moreover, we do not observe the (100) and (110) reflections.

From that two conclusions can be drawn: First, the PtSiTe structure, as well as any structure containing homoatomic dumbbells (Y_2 and Sn_2) can be ruled out for the investigated compounds as these would cause large distortions or layered structures as found in PtS_2 or PtSSe. Second, a disordered pyrite type as well as the ullmannite structure must be excluded for PtSnS and PtSnSe. The occurrence of the (100) and (110) reflections does not allow for centering and cubic symmetry, respectively. From the absence of these reflections in the case of PtSnTe we cannot conclude directly on ordering because Sn and Te are hardly to distinguish by X-ray diffraction. This was shown in the case of PtGeSe where the exchange of Ge and Se positions lead to the same R value for single crystal investigations [23]. It allows for a partly or fully disorder or even a ullmannite related ordering. However, the latter could not explain the orthorhombic distortion.

Summarizing we observe the necessary conditions for cobaltite type ordering in terms of orthorhombic distortions and the occurrence of the (100) and (110) reflections only for PtSnSe. In the case of PtSnS and PtSnTe the question arises if further models, or full or partial ordering are evidenced and if a clear preference of one structure is given that can be predicted systematically. Methods like Rietfeld refinement can

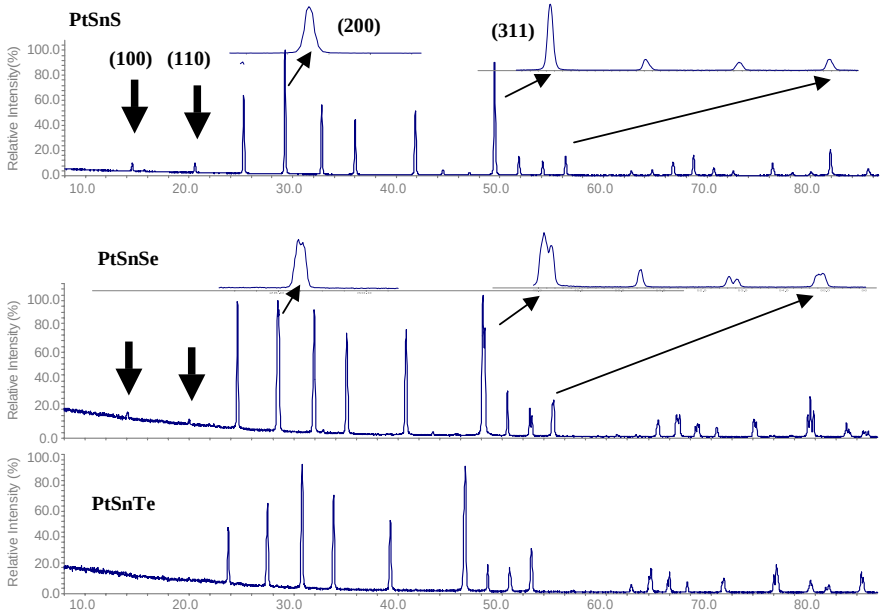

Fig. 2. Experimental diffraction patterns of PtSnS, PtSnSe and PtSnTe. The inlets show reflections like (200) with enlarged resolution. The indexing corresponds to pseudocubic cells.

give additional hints but all X-ray methods face the same problem that Sn and Te are hardly to distinguish. For detailed structure analyses single crystal investigations are currently in work.

The approach of the present work is to determine the preference of an ordering scheme from a systematic investigation that fits with experimental data as well as with crystallographic considerations. This should be applied in the same manner on the presented PtSnX compounds. A way is subsequently presented with an occupation scheme for *ab initio* modelling.

4. Modelling ordered variants of the PTS

4.1. Modelling scheme

We apply a model [24] to set up possible anionic ordering variants of the PTS that is an enriched version of [7,31]. It states that both the cobaltite ($Pca2_1$) and the ullmannite ($P2_13$, Fig. 3) structures can be represented as ordering variants in a symmetry reduced pyrite unit cell. Moreover, both are subgroups of the pyrite type structure. Thus, the ordered occupation of X positions in pyrite by X and Y fully determine their symmetry. In [7] the models are derived from a pyrite cell as ordering variants containing XY instead of XX entities. Two additional schemes with symmetry denoted as $P1$ and Pn are given. Here, we show that within the consequence of this scheme there are only three different ordered variants.

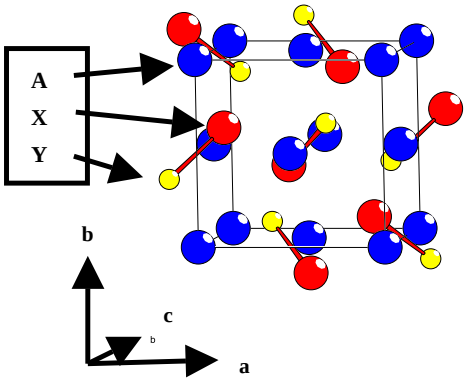

Fig. 3. Ullmannite structure, extended unit cell containing the counterparts of the XY dumbbells.

For an explanation we start from the unit cell of pyrite ($Pa\bar{3}$, no. 205) for MX_2 compounds that can be derived from the NaCl structure. Both M and X_2 entities form fcc substructures with X_2 in M_6 octahedral holes. The cubic symmetry is maintained by the X_2 entities where X occupies idealized 1/8 positions (Table 1). Thus, they are oriented along the space diagonals. The unit cell contains four X_2 entities ($Z = 4$). Fig. 4 shows the idealized X sites as multiples n of 1/8 projected along one lattice vector denoted as c perpendicular to the ab plane.

The possible values for $n = 1, 3, 5, 7$ are printed in the circles for the c axes. The occupation of half of the anionic sites by Y as illustrated in Fig. 4 and Table 1 now leads to XY entities. By each of the presented

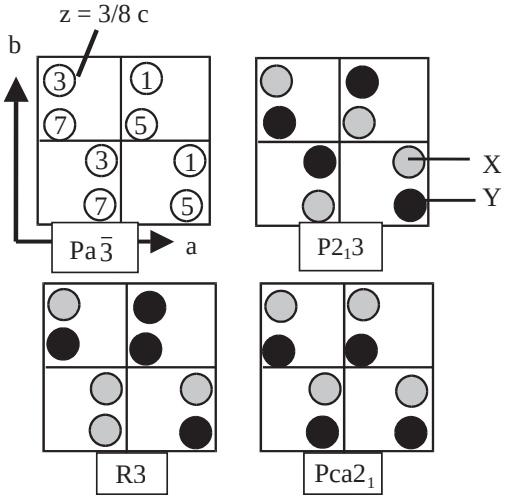

Fig. 4. Ordering schemes for anions X (gray circle) and Y (black circle) in 1/8 positions projected on the $a-b$ plane along c for (i) the PTS ($Pa\bar{3}$, top left), circled numbers denote the height along the crystallographic c-direction, (ii) the ullmannite (space group $P2_13$, top right), (iii) the rhombohedral structure ($R3$, bottom left), and (iv) the cobaltite structure ($Pca2_1$, bottom right).

Table 1
Occupation scheme of the anionic positions by $X-X$ and $X-Y$ dumbbells in pyrite and its ordering variants in an A-fcc sublattice (origin at A (0,0,0))

Anionic positions $(a/8, b/8, c/8)$	SG	Dumbbell 1		Dumbbell 2		Dumbbell 3		Dumbbell 4	
		333	555	571	317	157	731	715	173
$X-X$ in pyrite	$Pa\bar{3}$	$X1$	$X1'$	$X2$	$X2'$	$X3$	$X3'$	$X4$	$X4'$
$X-Y$ in ullmannite	$P2_13$	$X1$	$Y1$	$X2$	$Y2$	$X3$	$Y3$	$X4$	$Y4$
$X-Y$ in cobaltite	$Pca2_1$	$X1$	$Y1$	$X2$	$Y2$	$Y3$	$X3$	$Y4$	$X4$
$X-Y$ variant 1	$R3$	$Y1$	$X1$	$X2$	$Y2$	$X3$	$Y3$	$X4$	$Y4$
$X-Y$ variant 2	$R3$	$X1$	$Y1$	$Y2$	$X2$	$X3$	$Y3$	$X4$	$Y4$
$X-Y$ "$P1$" [7]	$R3$	$X1$	$Y1$	$X2$	$Y2$	$Y3$	$X3$	$X4$	$Y4$
$X-Y$ variant 4	$R3$	$X1$	$Y1$	$X2$	$Y2$	$X3$	$Y3$	$Y4$	$X4$

variants the local symmetry for the M atom changes from an angular distorted MX_6 octahedron with six equidistant $M-X$ (see [6,25]) in pyrite, to distorted MX_3Y_3 octahedra, where $M-X$ and $M-Y$ distances can differ. X and Y exhibit distorted tetrahedral coordinations XM_3Y and YM_3X.

A simple description of the possible symmetry lowering uses the orientation of the dumbbells: Describing the symmetry equivalent positions of X in pyrite as triplets $(a/8, b/8, c/8)$ the four dumbbells are: (333)–(555), (571)–(317), (157)–(731), (715)–(173). Replacing these four XX entities by XY results in three possibilities. There is only one scheme that gives a cubic symmetry, identified as the ullmannite structure. Its maximum symmetry is $P2_13$. Starting from here and exchanging the directions of two dumbbells a cell is received with the maximum symmetry of the space group $Pca2_1$, that represents the cobaltite type structure. An intermediate structure can be reached, when X and Y of only one dumbbell of either the cobaltite or ullmannite ordering scheme is exchanged. In that structure one threefold axis is maintained resulting in a rhombohedral cell with the maximum symmetry $R3$. This scheme shows that there are three and only three variants of anionic ordering for XY dumbbells replacing the XX entities in pyrite. It is the simple consequence of the relative orientation of four heteroatomic dumbbells along the four space diagonals of a metrically cubic cell. The ordering completely determines the respective maximum symmetry as $P2_13$, $Pca2_1$, or $R3$. This is in agreement with group–subgroup relations [26] as given in the International Tables for Crystallography [27]. In the line of this model observed lattice distortions and atomic displacements are restricted by and the result of the degrees of freedom given by a preferred ordering scheme imposed by short range ordering phenomena. A contrary model could state that long range effects in terms of lattice distortions impose preferred orientations of the dumbbells, or even that they are independent of their orientations at all.

4.2. DFT structure relaxations

With the use of the previously discussed scheme for an *ab inito* modelling we impose that the symmetry of the structure is completely determined by preferred relative orientations of four SnX entities, i.e. the ordered occupations of X sites with X and Y in a pyrite type unit cell. This allows for the optimization of each compound with respect to the ordering variant from one initial cell. We started from the ideally ordered structures, i.e. an fcc sublattice for Pt and 1/8 positions for Sn, Se, and Te as described in Section 3.2. Subsequently the atomic positions, cell size and shape were relaxed to find the corresponding energetic minimum.

Table 2
Results of the structure optimisations (full structure relaxations: volume, shape, and positions)

Space group	PtSnS E (meV)	PtSnSe E (meV)	PtSnTe E (meV)
I. $P2_13$ (198)	+23.20	+70.75	+103.79
II. $R3$ (146)	0.00	+14.15	+23.06
III. $Pca2_1$ (29)	+1.45	0.00	0.00

The results of the full structure relaxations, i.e. with respect to all degrees of freedom allowed by the ordering imposed symmetry are given in Table 2. From these results one finds that the energy differences are in the range of meV. However, the results follow a systematic way. For all compounds the ullmannite structure is the less favorable in total energy. The energy difference between the cobaltite and the rhombohedral structure is about one order of magnitude smaller and becomes closer from PtSnTe to PtSnSe and PtSnS. The preference of the cobaltite structure for PtSnSe and PtSnTe is given by the small amount of +14 and +23 meV, respectively. In the case of PtSnS the energy difference is even lower with the preference of the rhombohedral structure that was also found using a different code [28]. The very small energy differences in the range of meV determine the ordering of these compounds. It evidences thermally induced disorder as experimentally observed for CoAsS, where As and S are completely disordered above 800°C [29].

For our approach it is interesting to figure out if just the ordering leads to a preference or the ordering plus cell deformations. Thus, the atomic positions were relaxed keeping the cells metrically cubic at fixed cell sizes. In a second step both cell shape and atomic positions were allowed to relax at fixed volumes. By that we separated the influence of the lattice distortion and the ordering.

Fig. 5 shows the optimizations of PtSnS and PtSnSe for the steps 1 and 2, respectively. The curves denoted as $E29$, $E146$ and $E198$ relate the energy to the space groups of the respective ordering variants. We find for PtSnSe that indeed the ordering alone leads to the finally found energy order $E29 < E146 < 198$. Thus we conclude that the relative orientations of the SnX units determine the preference of the ordering. PtSnTe gives similar results.

Applying the same method for PtSnS the difference in energy between cobaltite like and rhombohedral ordering is about one order of magnitude lower than in PtSnSe. Both the $R3$ and the cobaltite variant of PtSnS are evidenced by a similar total electronic energy. From this result one can expect that both variants to occur in PtSnS crystals.

4.3. Structures and diffraction patterns

By the use of simulation tools [21] we calculated powder diffraction patterns for the structure models and

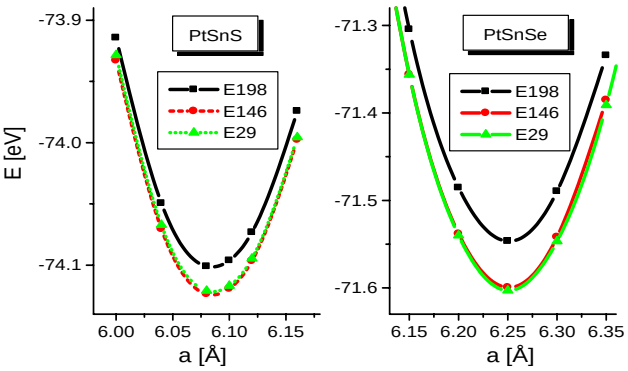

Fig. 5. Structure optimizations plotted as energy versus cell parameter a for PtSnS (atomic positions plus cell shape optimized) and PtSnSe (atomic positions free, metrically cubic cell fixed), see text.

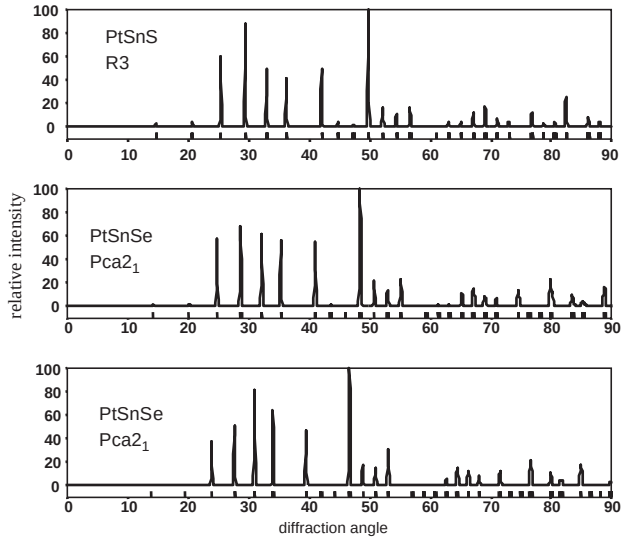

Fig. 6. Simulated powder diffraction patterns (for Cu radiation) for PtSnTe ($Pca2_1$, *m.*), PtSnTe ($Pca2_1$, bottom).

transferred the structures to the standard settings to give the atomic positions that are expected for X-ray investigations.

The simulated diffraction patterns (Fig. 6) for the three optimized models are in excellent agreement with the experimentally observed reflections. To point out again the (100) and (110) reflections are observed for the modelled variants of rhombohedral PtSnS and orthorhombic PtSnSe. They are not observed for PtSnTe although the cobaltite like ordering is given. This underlines the respective conclusion from the experimental part.

Comparing the cell parameters from the calculated and the results of the X-ray determinations one observes a slight underestimation of the cell volumes that is expected for LDA calculations. For the three ordered variants of PtSnS we observe a volume of 224.7 Å for the optimized structures, that is about 0.5% below the experimental value. The optimization of the rhombohedral cell results in a slight distortion of the rhombohedral angle to 90.09° that indeed fits with the observed splitting of high angle reflections (see Section 3.1). For all the orthorhombic models we predict lattice constants a, b, c that differ between 0.01 and 0.03 Å. This is again in agreement with experimental results on cobaltite type structures and it is distinguishable by powder diffraction. The cells of PtSnSe and PtSnTe are 8% and 20% larger than PtSnS, the densities slightly increase from 10.4 to 10.9 g/cm^3 (Table 3).

Further information on the ordering can be received, when we consider the local coordination in terms of interatomic distances (Table 4). Given by the structure type, Pt is coordinated by three Sn and three X (S, Se, Te) atoms in each case of the mentioned structure variants. As already pointed out, distinguishing the Ge and Se positions in PtGeSe turned out to be difficult [23] by X-ray diffraction. However, two different distances Pt–X and Pt–Y were found.

Our calculations on PtSnX give a similar result. For PtSnS the Pt–S distances are clearly found to be the shortest for all ordering variants around 2.45 Å. The Pt–Sn distances are the longest at 2.61 Å, and d(Sn–S) lies in between with 2.51 Å. Comparing the three models of PtSnS we observe that the $R3$ and the cobaltite structure allow for distortions of the coordination spheres. These lead to shorter Pt–S and longer Pt–Sn distances. These tendencies might explain the energy gain with the lowering of local symmetry. Comparing the Pt–Sn distances of PtSnSe and PtSnTe one observes an enlargement to 2.63 and 2.70 Å. With Pt–Se to Pt–Te the distances nearly reach the values of d(Pt–Sn). However, the increase of the $X-Y$ distance that becomes the largest with 2.85 Å in PtSnTe should be pointed out as a significant result. It means, that the strength of the bonding within the dumbbell decreases and the Pt–X bond becomes more important. This corresponds to observations on the $d(M-X)/d(X-X)$ relation pointed out on MX_2 systems from light to heavy PTS compounds like SiP_2 and $AuSb_2$ [25]. As the rhombohedral model describes a new structure type, an interesting feature should be pointed out here. Considering the second coordination spheres (>3 Å) tetrahedral holes of S_4 and Sn_4 are formed (Fig. 7) around the Pt atoms. Further work is needed to enlight whether this can have an effect on the stabilization of the rhombohedral structure.

4.4. Electronic band structure

The minimized structures were used to calculate their electronic band structures and densities of states (DOS). For all investigated compounds semiconducting behavior is predicted. This is proven by conductivity measurements (see Section 3.1). As known for the

Table 3
Lattice constants for PtSnS, PtSnSe and PtSnTe from X-ray diffraction and DFT calculations

	SG	V (Å^3)	a (Å)	b (Å)	c (Å)	$\alpha=\beta=\gamma$
PtSnS	$R3$	224.7	6.0795	6.0795	6.0795	90.09°
PtSnS	$Pca2_1$	224.7	6.0916	6.0847	6.0629	90.00
XRD		228.29(3)		6.1117(5)		90.00
PtSnSe	$Pca2_1$	242.3	6.2488	6.2387	6.2156	90.00°
XRD		244.9(1)	6.2744(13)	6.2597(15)	6.2351(14)	90.00
PtSnTe	$Pca2_1$	269.7	6.4761	6.4611	6.4457	90.00°
XRD		272.3(1)	6.4974(12)	6.4772(12)	6.4696(14)	90.00

Table 4
Interatomic distances for the calculated structures

	PtSnS	PtSnS	PtSnS	PtSnSe	PtSnTe
Space group	$P2_13$ (198)	$R3$ (146)	$Pca2_1$ (29)	$Pca2_1$	$Pca2_1$
d(Pt–X) (Å)	2.4580	2.4522, 2.4416, 2.4497, 2.4699	2.4429, 2.4514, 2.4626	2.5549, 2.5559, 2.5591	2.6532, 2.6548, 2.6594
d(Pt–Sn) (Å)	2.6093	2.6107, 2.6086, 2.6161, 2.6231	2.6062, 2.6211, 2.6216	2.6192, 2.6260, 2.6282	2.6884, 2.6924, 2.7032
d(X–Sn) (Å)	2.5216	2.5001, 2.5153	2.5070	2.6395	2.8417

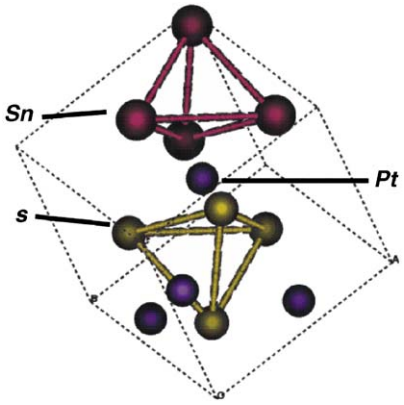

Fig. 7. Unit cell of rhombohedral PtSnS with the "Sn_4" and "S_4" holes outlined.

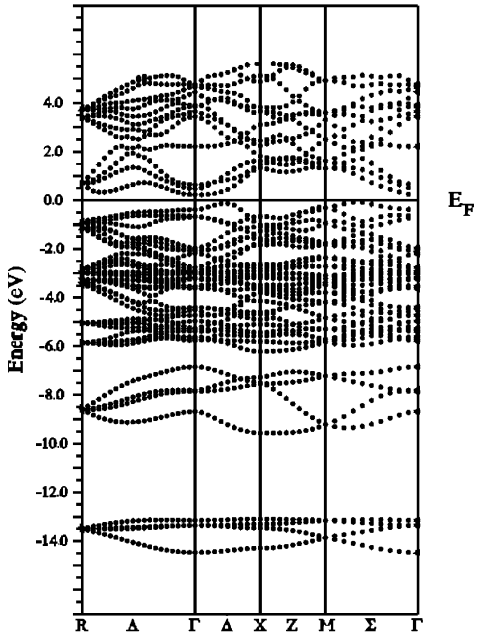

Fig. 8. Electronic band structure of PtSnSe from FP-LAPW-calculations on the optimized structure.

isoelectronic dipnictides [3] the band gap is indirect and becomes smaller with heavier elements [30].

As shown by the band structure of PtSnSe (Fig. 8) the valence band maximum (VBM) lies between Γ and X at Δ, as well as M and Γ at Σ, and the conduction band minima (CBM) at Γ. The calculated indirect gaps are 0.5 for PtSnS [24], 0.3 eV for PtSnSe, and 0.1 eV in the case of PtSnTe. These might be underestimated within the LDA. From the atomic site projected densities of states (PDOS, Fig. 9) one can observe strong mixing of all atoms at both the CBM and the VBM. The valence band can be distinguished into three parts where the DOS maximum between -2 and -4 eV contributes to Pt states. The upper (0 to -2 eV) and lower parts (-4 to -6 eV) are due to p-orbital interactions within the SnX dumbbells with considerable higher contributions of the chalcogen atoms. The chalcogen s-bands lie below -13 eV and Sn–s below -7 eV. Again, the relation to MX_2 pyrite type dipnictides as shown in [24,25] is indicated.

5. Summary and conclusion

The approach of this study was to model systematically the crystal structures and ordering preferences of PtSnS, PtSnSe and PtSnTe. We asked if it was possible to predict the correct ordering variant from *ab initio* as a

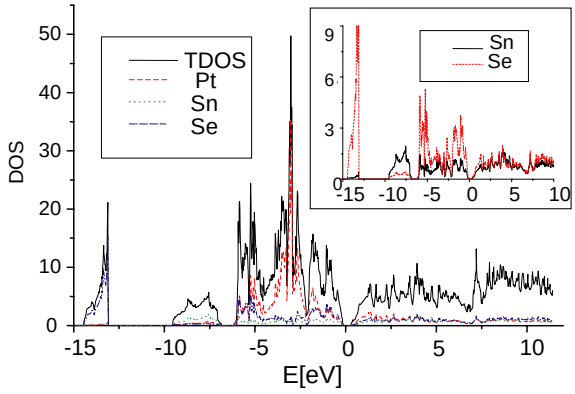

Fig. 9. Total and site projected density of states (TDOS, PDOS) for PtSnSe ($Pca2_1$), FP-LAPW calculation, the inlet shows the PDOS on the atomic orbitals of Sn (black) and Se (red).

step towards the understanding of the occurrence of different variants within the huge group of pyrite type related compounds with MXY stoichiometry. From nature the occurrence of two variants as the cubic ullmannite (NiSbS) and the orthorhombic cobaltite (CoAsS) are known for various compositions.

As the underlying concept well known scheme could be reduced and applied. The model is based on the fact that both the ullmannite and the cobaltite structure can be represented as ordered variants in a pyrite type unit cell. The ordered occupation of the anionic sites forming XY dumbbells completely determines the structural symmetry. From that concept a third variant of rhombohedral symmetry was derived and rationalized with the relative orientation of four XY dumbbells along the diagonals of a cube.

From powder diffraction patterns of PtSnS, PtSnSe, and PtSnTe one can conclude on the cobaltite type structure as claimed for the isoelectronic PtGeX. The appearance of the (110) and (100) reflections and the splitting of (200) excludes all variants but cobaltite type for PtSnSe. For PtSnS, that appears metrically cubic, and PtSnTe, where Sn and Te can hardly be distinguished by X-rays, , higher symmetry and rhombohedral distortions must be taken into account.

The first principle structure optimizations clearly result in the fact that the cubic ullmannite structure is the less favorable for the three compounds. Due to the total energy, PtSnTe and PtSnSe prefer the cobaltite structure, and PtSnS the rhombohedral type. The energy differences are in the range of meV. However, the lattice distortions predicted by the calculation agree with experimental findings, as well as the simulated diffraction patterns. The interatomic distances give reasonable results. The trend of longer and weakened Sn–X distances of the dumbbell agrees with known trends in the platinum dipnictides. The Pt–X distances are in all cases shorter than Pt–Sn. From band structure calculations we predict the compounds to be indirect semiconductors with a low gap that becomes smaller from PtSnS (0.5 eV) to PtSnSe (0.3 eV), and PtSnTe (0.1 eV).

Thus, the shown approach does distinguish the ordering variants and gives reasonable results. It can be applied on similar systems especially PtGeSe, where X-rays fail and new compounds for crystal engineering. It can serve as a basis for further systematic work on bonding properties like polarization, charge transfer and related phenomena. The small energy differences especially calculated for PtSnS serve as a challenge for future experimental work on single crystals to prove the existence of the rhombohedral structure or even a coexistence with the cobaltite type. Thus, experiment and modelling come together to enrich the understanding of ordering phenomena, as intended by this paper.

Acknowledgments

Special thanks is given to Prof. Dr. Arno Pfitzner, Dr. Martina Andratschke, Dr. Manfred Zabel, Daniela Feil, Ulrike Schiessl, and Andreas Strasser for the support of the sample preparations and investigations as well as to the supercomputer center m3pec at the University Bordeaux1. The calculations have been carried out on the IBM Regatta machine at m3pec.

References

[1] F. Hulliger, Nature 198 (1963) 382.
[2] A.J. Foecker, W. Jeitschko, J. Solid State Chem. 162 (2001) 69.
[3] F. Hulliger, Nature 200 (1963) 1064.
[4] N.E. Brese, H.G.v. Schnering, Z. Anorg. Allg. Chem. 620 (1994) 393–404.
[5] W.I. Bragg, Proc. Roy. Soc. of London A 89 (1914) 468.
[6] R. Weihrich, V. Eyert, S.F. Matar, Chem. Phys. Lett. 373 (2003) 636.
[7] P. Entner, E. Parthé, Acta Crystallogr. B 29 (1973) 1557.
[8] Y. Barkov, R.F. Martin, R.J. Kaukonen, T.T. Alapieti, Can. Mineralog. 39 (2001) 1397.
[9] J.L. Jambor, A.C. Roberts, Am. Mineral. 87 (2002) 996.
[10] P. Villars, L.D. Calvert, Pearson's Handbook of Crystallographic Data, American Society for Metals. 2nd Edition, Vol. 4, ASM International, Materials Park, OH, 1991.
[11] M.F. Mansuetto, J.A. Ibers, Z. Kristallogr. 209 (1994) 708.
[12] G. Kresse, J. Furthmueller, Phys. Rev. B 54 (1996) 11169.
[13] G. Kresse, J. Hafner, J. Phys.: Condens. Matter 6 (1994) 8245.
[14] P. Pulay, Chem. Phys. Lett. 73 (1980) 393.
[15] H.J. Monkhorst, J.D. Pack, Phys Rev B 13 (1976) 5188.
[16] P.E. Bloechl, O. Jepsen, O.K. Andersen, Phys. Rev. B 49 (1994) 16223.
[17] D. Hobbs, J. Hafner, J. Phys.: Condens. Matter 11 (1999) 8197.
[18] H. Toulhoat, P. Raybaud, S. Kasztelan, G. Kresse, J. Hafner, Catalysis Today 50 (1999) 629.
[19] P. Blaha, K. Schwarz, G.K.H. Madsen, D. Kvasnicka, J. Luitz, Wien2k, An Augmented Plane Wave + Local Orbitals Program for Calculating Crystal Properties, 2001.

[20] J.P. Perdew, A. Zunger, Phys. Rev. B 23 (1981) 5048.
[21] Cerius^2 simulation package, Molecular Simulations Inc., San Diego, 1997.
[22] M. Fleet, P.C. Burns, Can. Mineral. 28 (1990) 719.
[23] S.C. Abrahams, J.L. Bernstein, Acta Crystallogr. B 33 (1977) 301.
[24] R. Weihrich, Ph.D. Thesis, Regensburg, 2002.
[25] A.C. Stueckl, R. Weihrich, K.-J. Range, Frontiers of Solid State Chemistry, Proceedings of the International Symposium on Solid State Chemistry in China, Changchun, 2002, p. 117.
[26] H. Baernighausen, MATCH 9 (1980) 139.
[27] T. Hahn, International Tables For Crystallography, 5th Edition, Vol. A, Kluwer Academic Publishers, Dordrecht, 1995.
[28] M.C. Payne, M.P. Teter, C.C. Allan, T.A. Arias, J.D. Joannopoulos, CASTEP 4.2, academic version, Rev. Mod. Phys. 64 (1992) 1045.
[29] R.F. Giese, J.R. Kerr, P.F. Kerr, Am. Mineral. 50 (1965) 1002.
[30] D. Dai, H.-J. Koo, M.H. Whangbo, C. Soulard, X. Rocquefelte, S. Jobic, J. Solid State Chem. 173 (2003) 114.
[31] P. Bayliss, Can. Mineral. 24 (1986) 27.
[32] S.C. Abrahams, J.L. Bernstein, E. Buehler, Mater. Res. Bull. 11 (1976) 707.